JOURNAL OF AIRCRAFT
Vol. 31, No. 4, July–Aug. 1994

Turbulent Flow Structure Associated with Vortex-Induced Fin Buffeting

Christian Breitsamter* and Boris Laschka†
Technische Universität München, 80290 Munich, Germany

Selected results from an extensive experimental investigation showing the flowfield in the fin region of a delta-canard-configuration are presented. Results obtained include detailed flowfields of the time-dependent velocity components for various angles of attack (0–31.5 deg) at a test Reynolds number of 1.0×10^6 using hot-wire anemometry. The structure of the highly turbulent vortex dominated flow is clearly shown by time-averaged, root-mean-square (rms) and spectral distributions. Thus, strong interference effects between the canard and the wing vortex systems around the fin region are found. With increasing incidence the wing and the canard leading-edge vortices move inboard resulting in an increase of the velocity fluctuations in the area of the midsection. The power spectral density depicts significant frequency peaks related to the concentration of kinetic turbulent energy in the flow of the wing/canard vortex sheet. At high incidences the narrow-band turbulent energy induced by the vortex sheet affects the plane of symmetry because of the shift of the leading-edge vortex. This substantiates that fin oscillations at high-α are excited by narrow-band fluctuations due to vortical flow conditions.

Nomenclature

f	=	frequency, Hz
k	=	reduced frequency, fl_μ/U_∞
l_μ	=	wing mean aerodynamic chord
Re	=	Reynolds number, $U_\infty l_\mu/\nu$
s	=	wing half-span
U_∞	=	freestream velocity
u, v, w	=	streamwise, lateral, and vertical velocity
$\bar{u}, \bar{v}, \bar{w}$	=	streamwise, lateral, and vertical mean velocity
u', v', w'	=	fluctuation part of u, v, w
$u_{rms}, v_{rms}, w_{rms}$	=	rms values of the fluctuating components of velocity, $u_{rms} = \sqrt{\overline{u'^2}}$, $v_{rms} = \sqrt{\overline{v'^2}}$, $w_{rms} = \sqrt{\overline{w'^2}}$
$u_{xz_{rms}}$	=	rms value of the streamwise and vertical fluctuating components
x, y, z	=	streamwise, lateral, and vertical coordinates of the wind-tunnel axis system
Y, Z	=	nondimensionalized coordinates in the measurement plane, referred to s, origin at the midsection
α	=	aircraft angle of attack
Λ	=	wing aspect ratio
λ	=	wing taper ratio
ν	=	kinematic viscosity
φ_C	=	canard leading-edge sweep
φ_W	=	wing leading-edge sweep

Introduction

MODERN high-agility aircraft of canard-delta wing type may generate leading-edge vortices which produce substantial increases in lift. This is utilized to achieve enhanced maneuverability at high angles of attack. Aircraft structures under such flow conditions are subject to random aerodynamic loads arising from the impact of vortical flows on the structures, in particular, when vortex bursting occurs.

An example of this type of severe aerodynamic loading is the phenomenon of fin buffeting. It is characterized by irregular oscillations of the airplane or its components induced by flow separation.[1] The oscillations occur normally in the vicinity of the natural frequencies of the system.[2] Buffeting can be treated analytically as a dynamic aeroelastic response problem complemented by the self-induced aerodynamic forces which provide usually damping. At the present time, the knowledge of the buffeting excitation spectrum can only be obtained from experimental data. Measurements[3] have shown that the spectrum of the separated flow region behind a wing may have distinct peaks at certain frequencies in which the kinetic turbulent energy is concentrated.

Fin-buffeting has inspired many studies on leading-edge vortex-producing configurations,[4] and recently emphasis on the twin-tail buffeting problem[5] (F/A-18, F-15) has increased. The recorded data consist of mean and unsteady forces and moments,[6] steady and unsteady field and surface pressure measurements,[7,8] flow visualization of the vortex structure,[9] water-tunnel experiments on vortex bursting,[10] and small-scale wind-tunnel fin pressure measurements and vertical tail acceleration data from flight test.[11] Flow measurements around a model of a YF-17 highlight the dominance of vortices emanating from leading-edge extensions.[12] It was shown that the bursting of these vortices effects large velocity fluctuations at the vertical tails. A quantitative study on the low-speed flow environment of small-scale models of a F-15 presented peaked velocity spectra inboard and outboard of the vertical tails at high incidence.[13,14] Narrow-band velocity fluctuations even in the absence of strong vortices were observed.

For the particular case of fighter-type aircraft, characterized by thin, highly swept wings, the flow separates quite close to the leading edge regardless of Reynolds number. Also, most maneuvers at high incidence are associated with low Mach numbers due to structural limitations. That means that the effects of compressibility are not primary issues. Data obtained at different Reynolds and Mach numbers may be influential,[9] due to the effects of surface roughness, tunnel turbulence, wall effects, and model support interference.

Methods for predicting wing response to buffet loads were evaluated.[15,16] Reference 17, presenting a method based on wind-tunnel data, shows that buffet spectra could be extrapolated over large ranges of velocity, and model size, and that

Received Dec. 31, 1992; revision received June 23, 1993; accepted for publication July 6, 1993.

*Dipl.-Ing., Research Engineer, Lehrstuhl für Fluidmechanik, Arcisstr. 21.

†Professor Dr.-Ing., Full Professor of Fluid Mechanics, Lehrstuhl für Fluidmechanik, Arcisstr. 21.

they could be used to predict flight loads. Lan et al.[18] developed an analytical method to generate a fluctuating flowfield producing unsteady pressures due to vortex breakdown. This method is based on test data of the mean square values of fluctuating normal forces. Therefore there is a strong need for the measurement of the fluctuating velocity components in a buffeting inducing flowfield.

At present there is a lack of detailed instantaneous flowfield data to evaluate a more general understanding of fin buffeting. As a contribution to fill this gap, a research program on a typical high performance aircraft model was initiated at the Institute of Fluid Mechanics of the Technical University Munich.

In this article emphasis is on the knowledge of the turbulent flow structure behind leading-edge vortex dominated configurations causing fin buffeting. The approach adopted here is to measure the fluctuating velocity components in the fin region. Statistical analysis will be applied to show whether a significant frequency is present in the flow of burst vortices. The next step will be to look if flowfield frequencies are close to the natural frequencies of the fin. It should support the development of computational methods for prediction of tail buffeting.

Experimental Technique and Test Program

Facility and Model Description

The experiments were carried out in a 1.5-m low-speed wind tunnel. It has an open test section, its length is 3 m; maximum usable velocity is 55 m/s. Turbulence intensity ranges from 0.3 to 0.4% over the speed range of interest. The tunnel is equipped with an automated data acquisition and control system using a personal computer. Online data transfer and communication with a CONVEX C1 is utilized for data storing, reduction and processing by statistical means.

The model used is a very stiff model of a delta-canard configuration. A two-view sketch is presented in Fig. 1. For these tests, the canard setting angle has been fixed at zero deg. The model was sting-mounted on its lower surface using a computer controlled moving support strut providing an incidence range from 0–31.5 deg.

Hot-Wire Anemometry

The hot-wire probes are operated by a DISA C three-channel, constant-temperature anemometer system. Signal conditioner modules transform the bridge output voltages into a suitable range for the 16-channel simultaneous-sampling 12 bit A/D converter of the personal computer. The total sampling frequency is limited to 130 kHz. Crosswire probes (DISA 55A32 and 55P61) were used to measure the magnitude and the associated direction of the time-dependent velocity vector. The sensors consist of 5-μm-diam platinum-plated tungsten wires giving a length/diameter ratio of 250. The wires form a measuring volume of approximately 0.8 mm in diam and 0.5 mm in height. The sensor angle of 45 deg was chosen assuming that the best angular resolution will be obtained with pairs of perpendicular wires. An additional temperature probe is used to correct the anemometer output-voltages if ambient flow temperature varies.

For calibration of the hot-wire probes a computer-aided fully automated procedure is developed based on a velocity- and flow-angle-dependent, temperature corrected method.[19–23] In order to fully determine all three velocity components (u, v, w) the probe has to be rotated around its axis by 90 deg to adjust the wire plane (once horizontal and once vertical) against the main flow direction. Thus, two traverse sweeps are necessary to obtain the streamwise u, lateral v, and vertical w components, respectively.[23]

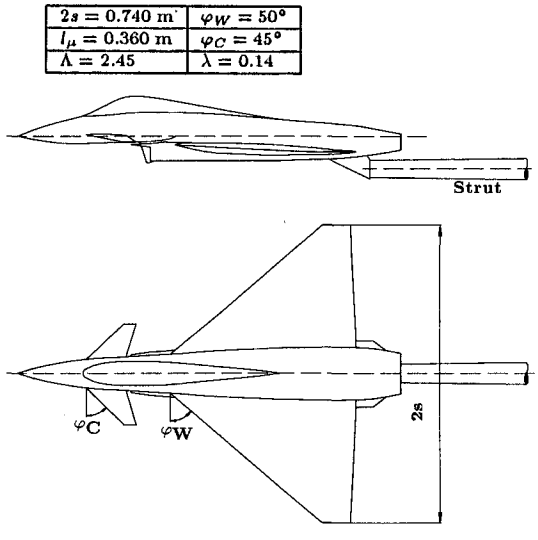

Fig. 1 Model of the delta-canard configuration.

Description of the Tests

Flowfield measurements were made in a plane perpendicular to the model x axis at a possible single or twin-fin location (Fig. 2). The tests were made for seven angles of attack (0, 15, 20, 25, 28, 30, and 31.5 deg) at a freestream reference velocity U_∞ of 40 m/s. This gives a Reynolds number of approximately $Re = 1.0 \times 10^6$ based on the wing mean aerodynamic chord for all the results presented. Because the wing leading edge was sharp, free transition was used.

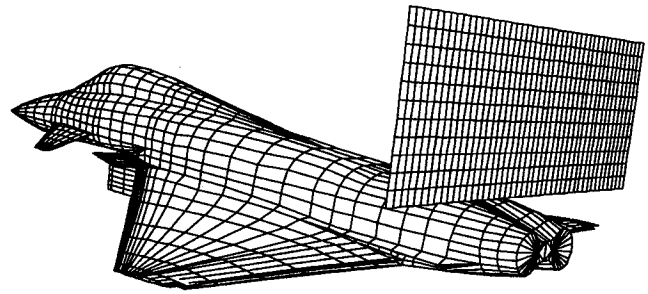

Fig. 2 Location of the measurement plane.

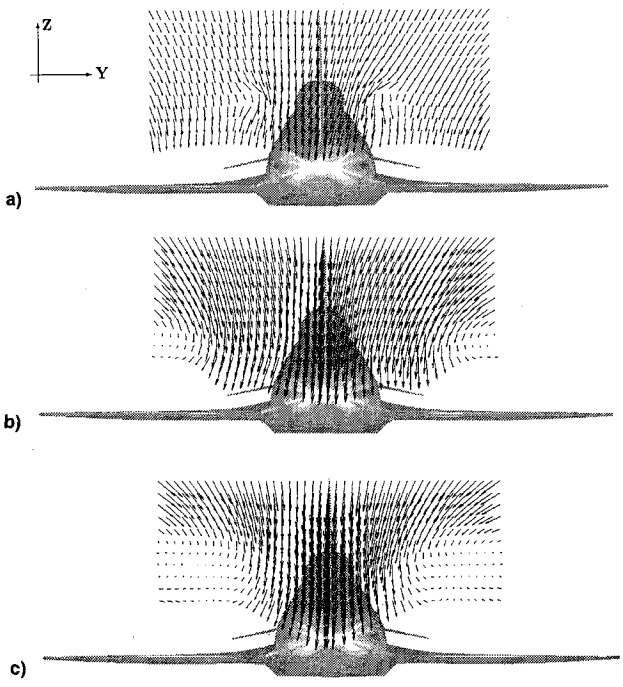

Fig. 3 Crossflow vectors in the measuring plane at α = a) 15, b) 20, and c) 30 deg.

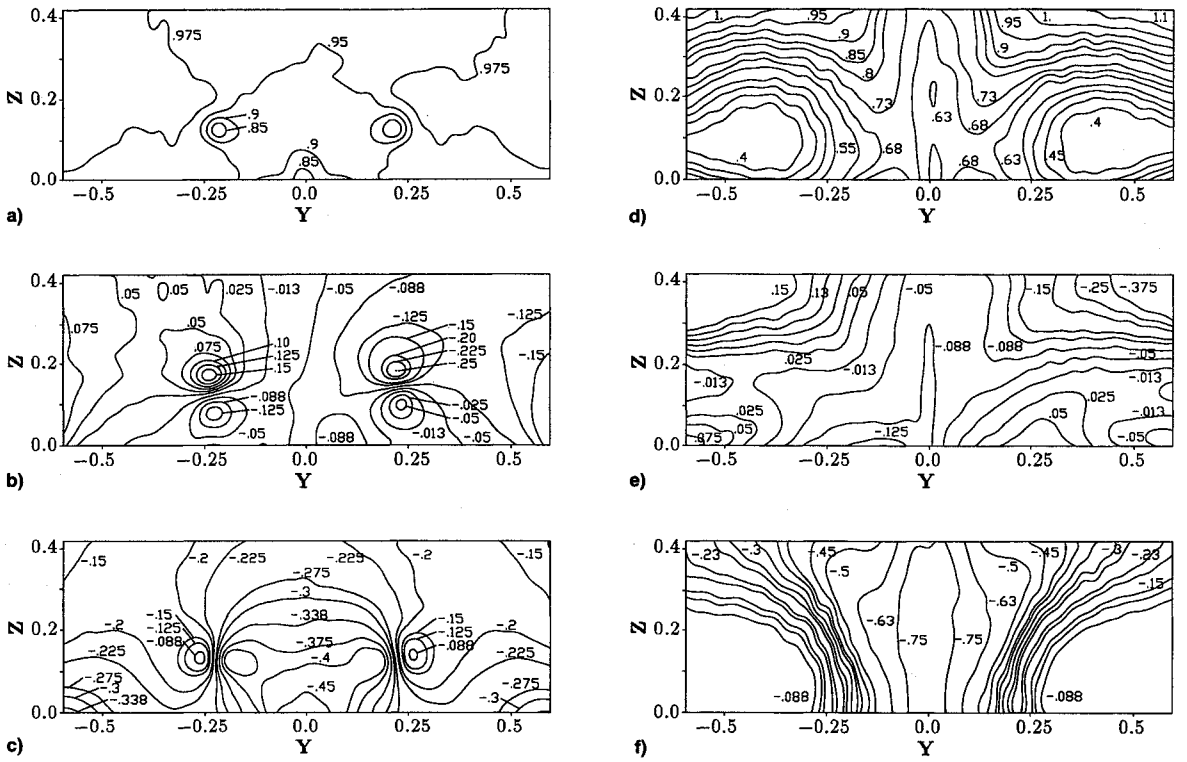

Fig. 4 Contours of mean velocity: a) $\bar{u}/U_\infty$, b) $\bar{v}/U_\infty$, and c) $\bar{w}/U_\infty$ of the left figure at $\alpha = 15$ deg and d) $\bar{u}/U_\infty$, e) $\bar{v}/U_\infty$, and f) $\bar{w}/U_\infty$ of the right figure at $\alpha = 30$ deg.

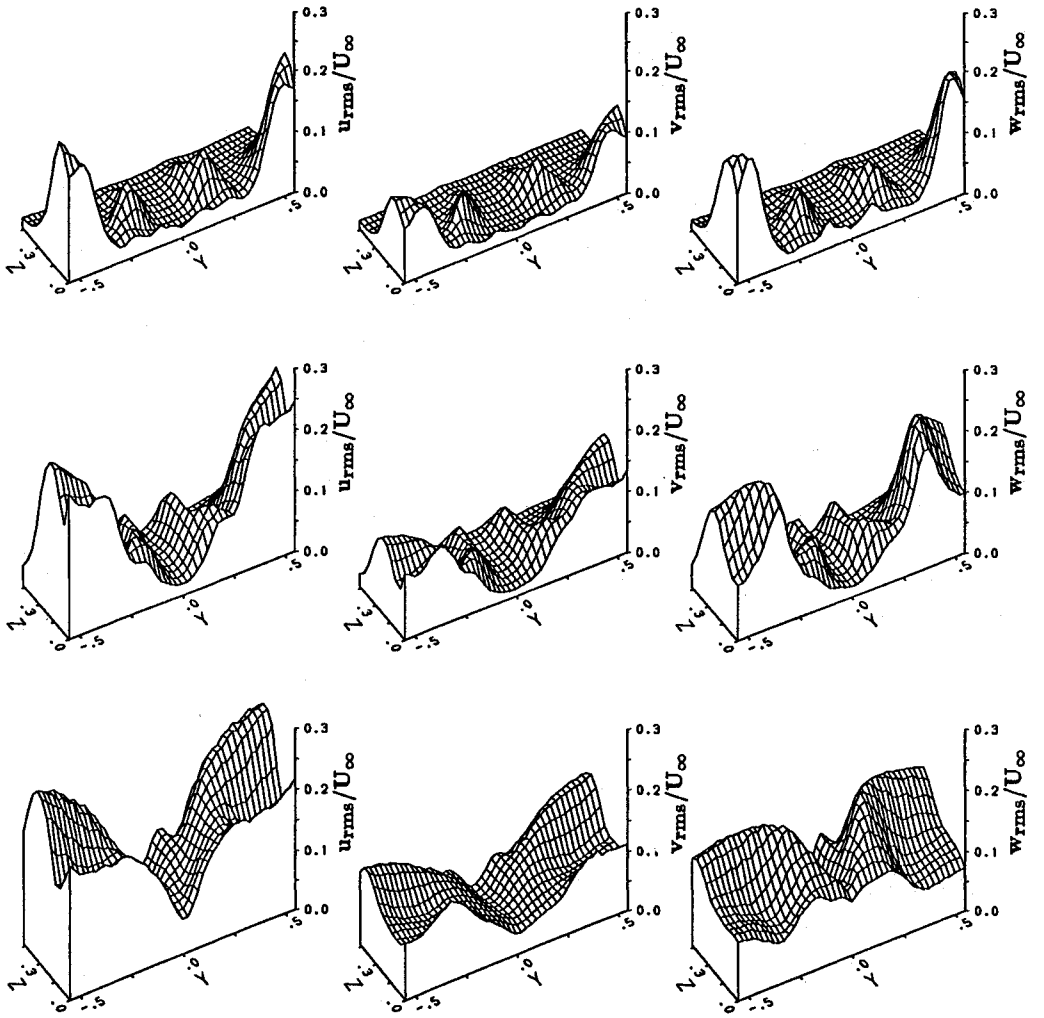

Fig. 5 Carpet plots of streamwise, lateral, and vertical rms velocity, u_{rms}/U_∞, v_{rms}/U_∞, w_{rms}/U_∞, at α = a) 20, b) 25, and c) 31.5 deg.

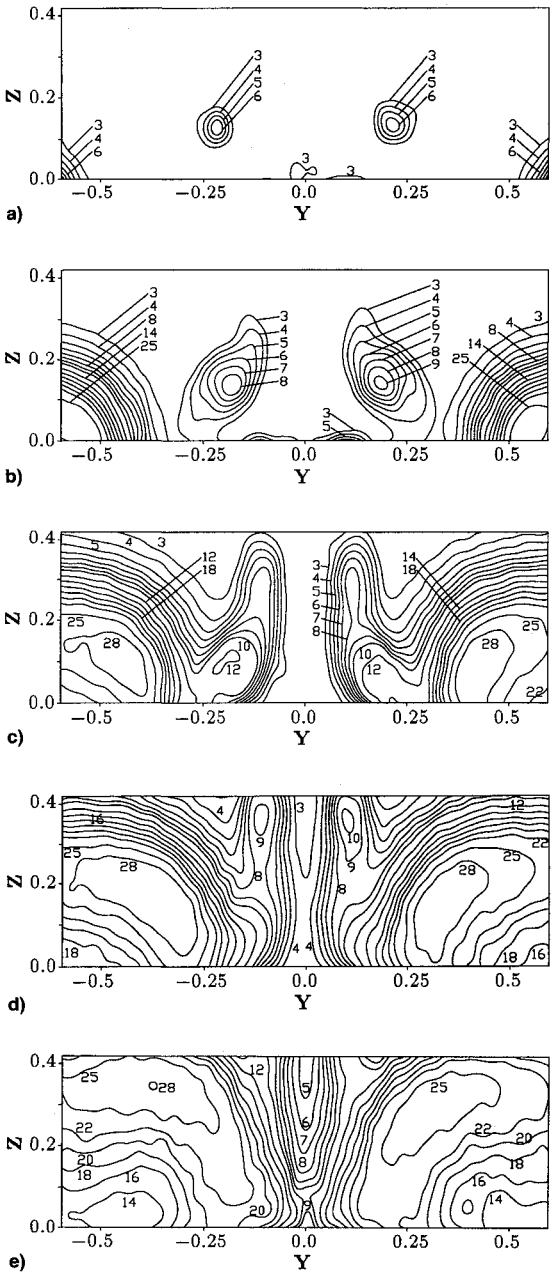

Fig. 6 Root-mean-square velocity contours $u_{xz_{rms}}/U_\infty$ (sum of streamwise and vertical component) at α = a) 15, b) 20, c) 25, d) 28, and e) 31.5 deg (values in percent).

The sampling frequency for each channel was set to 3 kHz. The anemometer signals were low-pass-filtered at 1 kHz before digitization to counter the aliasing effect. This is due to the check that no other significant flowfield phenomena are present in the higher frequency domain. The sampling time for each measuring point is 26.4 s depending on stable, time-averaged auto-spectra due to the turbulent flow structures. Based on the fundamentals of random error evaluation methods,[24] accuracies of 0.2, 1, and 3% are desired for the mean and standard deviation and the spectral density, respectively.

A typical survey plane contained 45 evenly spaced points spanwise and 11 evenly spaced points vertically (Fig. 2), giving a grid resolution of 0.014 in the spanwise and 0.020 in the vertical direction based on the wing span. The measurements were performed with and without a single fin to get information about the influence of the fin itself on the formation of the vortex dominated flowfield.

Results given in this article are for the fin-off case only. The fin-on case has not shown significant differences in the time-averaged and rms velocity distributions. The mounted fin produces only a small displacement effect on the core positions of canard and wing vortices due to 0.5–1.5% of the wing span. Reference 25 contains the complete results of this investigation.

Results and Discussion

Mean Velocity Distributions

Figure 3 gives a general view about the development of the vortex-dominated flowfield from moderate to high angle of attack showing the crossflow ($\bar{v}$, $\bar{w}$) velocity vectors. In addition Fig. 4 shows contours of mean velocities $\bar{u}/U_\infty$, $\bar{v}/U_\infty$, $\bar{w}/U_\infty$ for α = 15 and 30 deg.

The flowfield of the measurement plane is characterized by the interaction of several vortex systems, mainly produced by the canard and the delta wing. Figure 3a, α = 15 deg, shows that the flowfield is mainly influenced by the delta-wing primary vortices. They induce strong additional spanwise and downward velocity components. The canard vortices can be clearly identified in the lower part of the measuring plane near the fuselage. The local upwash from the canard vortex system is suppressed by the superimposed downwash field of the wing leading-edge vortices. The quantities of the corresponding velocity components may be taken from contours of Figs. 4a–4f. The axial velocity $\bar{u}$ in the core of the canard vortex system has decelerated to approximately 85% of the freestream value. This considerable decrease in the canard vortex core indicates that even for moderate angles of attack the vortices are strongly influenced by viscous effects. Consequently, the shape of the velocity field of the core is quite different from that of a potential vortex.

The wing's primary vortices move inboard towards the fuselage and upwards above the wing when the angle of attack is increased, Figs. 3b and 3c. The flowfield is then completely dominated by the wing leading-edge vortices. With higher angle of attack the intensity of the vortex induced crossflow velocities has increased. Because of the strong inward and downward velocity the canard vortex system cannot be resolved any more. Severe flow deceleration occurs at the lower edges of the measuring plane, resulting in strong velocity gradients. The change from flow acceleration to deceleration is evident due to the bursting of these vortices.

The delta-wing vortices are already burst over the wing at α = 8 deg. This has been taken from surface flow visualization tests.[26] Bursting over the wing occurs on a simple 50-deg swept-delta wing at $\alpha \geq 10$ deg. Because of the canard downwash, the wing leading-edge vortices develop progressively[27] due to the lower effective angle of attack at inboard locations. However, the model used here has a nonplanar wing which is strongly curved upwards near the fuselage. This is associated with an angle-of-attack increase in the region behind the canard. Thus, the canard downwash does not delay the vortex bursting over the wing.

At α = 30 deg, the burst wing vortices increase further in their radial extension leading to a big vortex core. This inner part of the vortex is characterized by very small velocity components (Figs. 4d–4f). The increase of the vortex core is connected with the decrease of velocity to meet the continuity equation, but it is obvious that strong viscous effects dominate the flow in a rather large area around the center of the primary vortex. Although the core becomes very large, a well-structured swirling flow pattern can be observed around it. When the angle of attack is increased, the borders of the primary vortices move closer together. In connection with the induced circumferential velocities, a nozzle effect appears in the midsection (Fig. 4f).

Root-Mean-Square Velocity Distributions

The turbulent flow structure is quantified by the rms values of the velocity fluctuations. Figure 5 presents carpet plots of the rms distribution for all three velocity components. Figures 6 and 7 contain the rms contours.

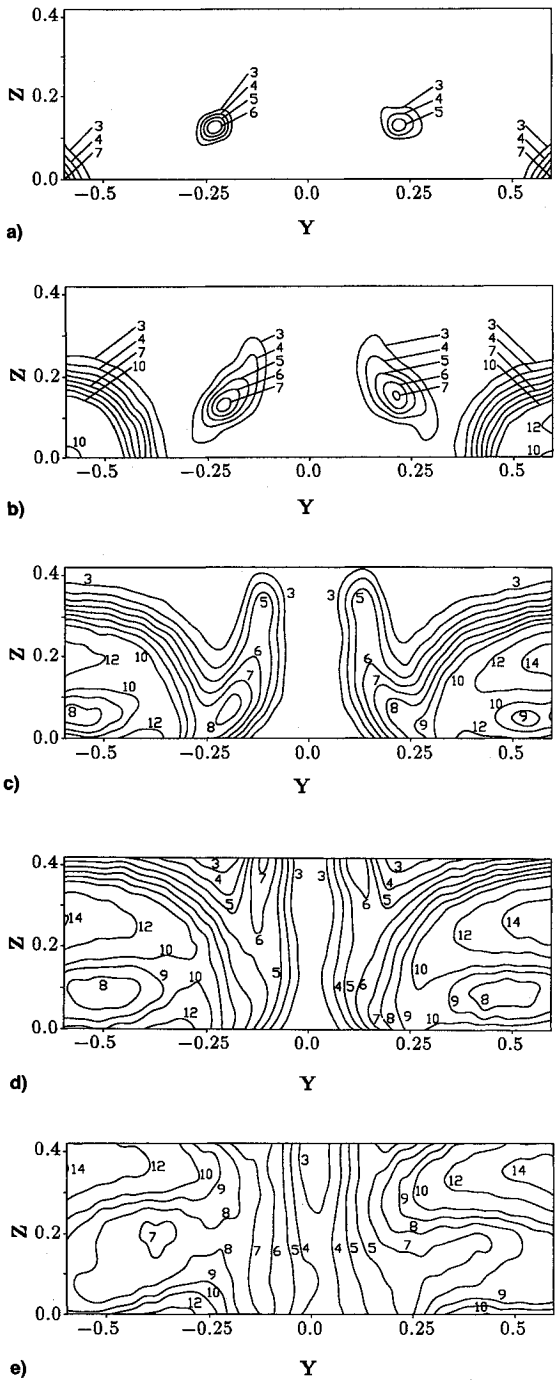

Fig. 7 Root-mean-square velocity contours v_{rms}/U_∞ at α = a) 15, b) 20, c) 25, d) 28, and e) 31.5 deg (values in percent).

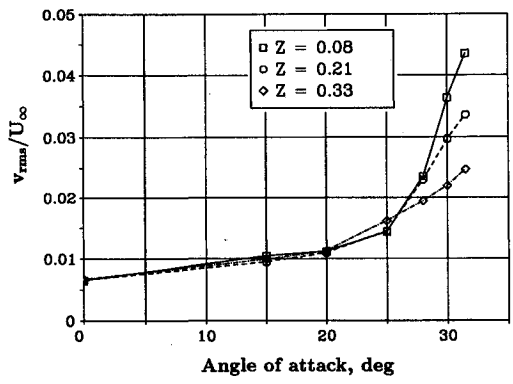

Fig. 8 Lateral rms velocity as a function of angle of attack at various distances above the surface.

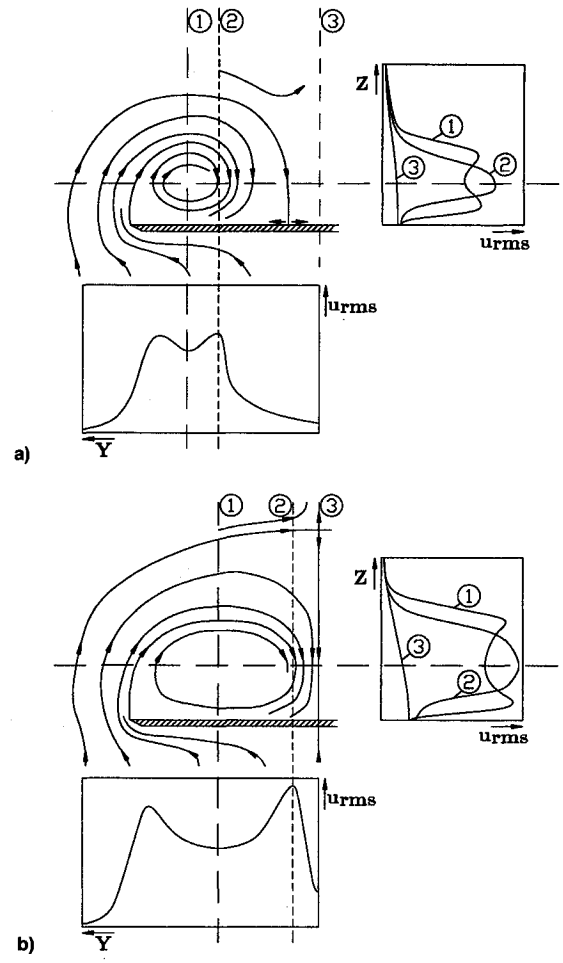

Fig. 9 Schematic overview of the steady and unsteady flowfield velocity for moderate and high angles of attack. Transverse flowfield and rms profiles at $\alpha \approx$ a) 15 and b) 30 deg.

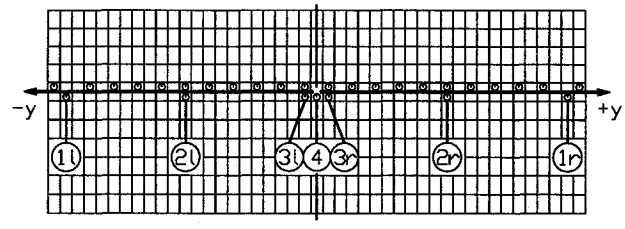

Fig. 10 Measurement stations for velocity spectra.

Figure 5a shows the rms distribution at α = 20 deg. The canard leading-edge vortices are indicated by local rms humps of approximately 8–10% around the midsection. This is consistent with the axial velocity drop seen in Fig. 4a and with the velocity jumps of Figs. 4b and 4c, respectively. There is also an evident increase in the fluctuation intensity at the lower cross section edges which are related to the wing primary vortex sheets as well as very steep gradients in the rms distribution in the sheet itself. This corresponds to the sharply marked off vortex core of strong flow deceleration (Fig. 4). The maximum rms values reach levels of approximately 21%. In the upper part of the measurement plane only the level of freestream turbulence exists.

At α = 25 deg (Fig. 5b), the turbulent region has grown considerably in both size and strength. The lower part of the measuring plane is dominated by large rms values for all three velocity components which are due to the wing primary and the canard vortex sheets.

As mentioned before (Fig. 5a), the canard vortex system is indicated by local rms maxima near the midsection. With increasing angle of attack the canard vortex system passes the

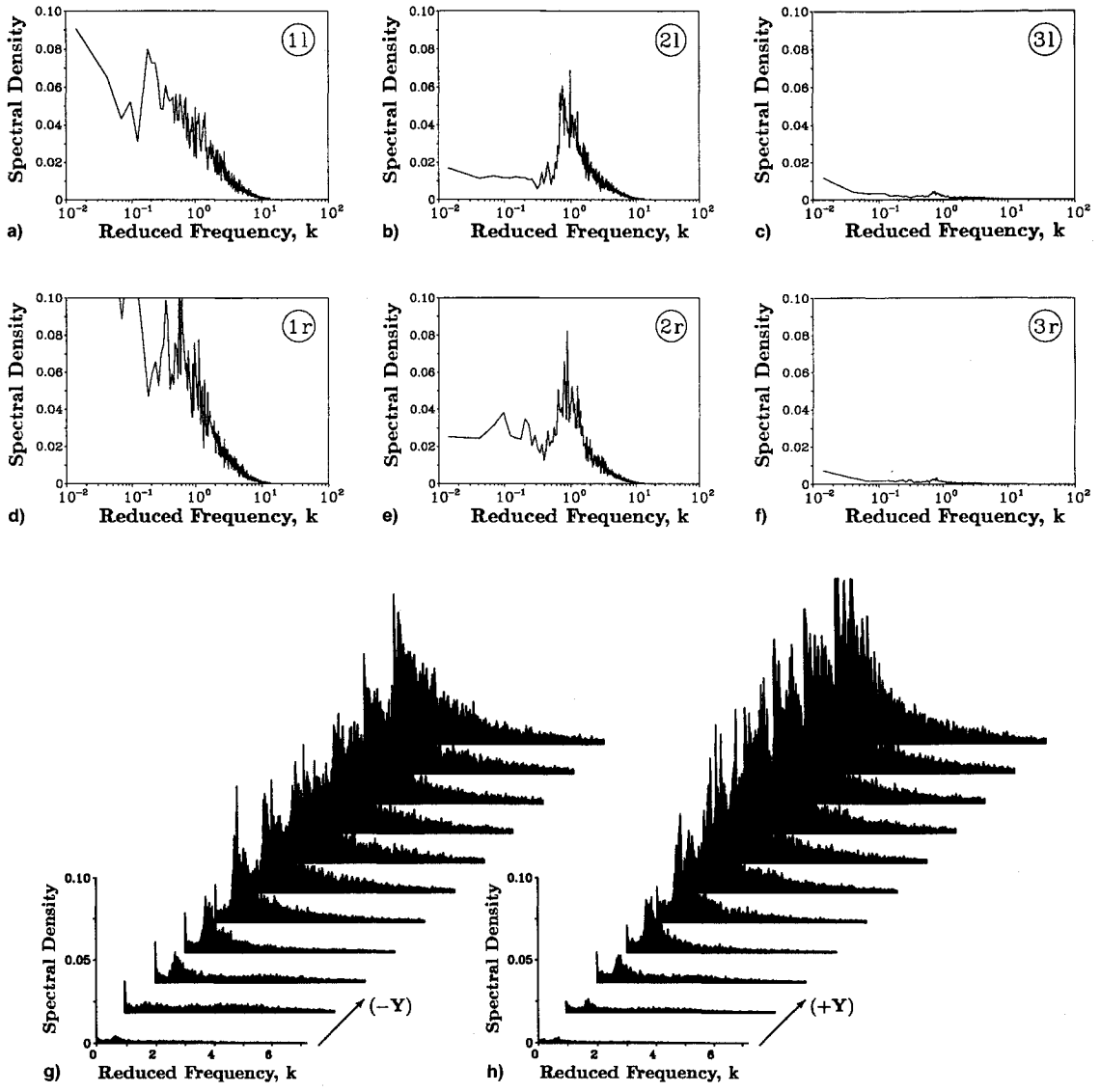

Fig. 11 Spectra of the lateral velocity component v, left and right of the plane of symmetry at $Z = 0.21$ and $\alpha = 28$ deg. v_{rms}/U_∞ = a) 12.4, b) 10.1, c) 3.0, d) 13.9, e) 10.7, and f) 2.4%; parts g) and h) are spectra of the left side ($-Y$) and right side ($+Y$), respectively.

wing leading edge relatively high above the wing. It consists of the canard's leading-edge and its trailing-edge vortex. This vortex system keeps its structure downstream still behind the wing trailing edge.[25] From the comparison of Figs. 6a and 7a ($\alpha = 15$ deg) and Figs. 6b and 7b ($\alpha = 20$ deg), it can be inferred that through wing influence the canard vortex system is moved above the wing inward towards the fuselage and also downward towards the wing surface. At 25-deg angle of attack the interaction between the vortex systems of the wing and the canard is such that the canard vortex sheet belonging to the trailing vortex starts to move upwards away from the wing while the canard leading-edge vortex is moved inwards and downwards to merge with the sheets of the wing primary vortices.

With a further increase to $\alpha = 28$ deg, the rms values of all three components become still larger again (Figs. 6d and 7d). The canard leading-edge vortex sheets are completely merged in the wing leading-edge vortices. The upper part of the canard's vortex system referring to the trailing-edge vortices remains separate from the wing's primary vortex sheets. The maxima of the rms velocity fluctuations go up to 31, 15, and 28% for the u, v, and w components, respectively.

The vortex regions of the wing primary vortices reveal that the maxima of the rms velocities are concentrated in an annular structure around the core. It is related to the vortex sheet (shear layer) due to the swirling pattern. However, the inner part of the core has a decrease in local rms. The reason for lower rms values in the core is the loss of mean velocity as well as the low velocity gradient within the core which reduces the turbulence level. The very steep gradients of the vortex sheet's rms distribution outside the core do not change with increasing angle of attack.

Although at $\alpha = 31.5$ deg (Figs. 6e and 7e) the maximum rms values of the velocity fluctuations have not grown considerably, their region of influence has. There is an increase to much higher rms values in the midsection which is caused by the inward shift of the wing primary and combined canard vortex sheets. This explains the severe increase of lateral rms velocity fluctuation in the midsection at high-α flow conditions. By comparison with the outboard region (vortex sheet and core) the midsection shows the lowest turbulence level. The lower turbulence level is also due to flow acceleration between the two wing leading-edge vortices.

Figure 8 presents the turbulence level of the v component for three vertical stations in the plane of symmetry as a function of the angle of attack. The rms levels increase from 0.7% at $\alpha = 0$ deg to 4.5% at $\alpha = 31.5$ deg. A significant rise starts at $\alpha = 25$ deg when the primary vortex approaches the plane of symmetry. The maximum rms value appears at the lowest vertical station at $\alpha = 31.5$ deg, at the wing midsection. Here, the wing primary vortex sheet has merged with that of the canard leading edge. The latter is shifted to the lower part of the midsection.

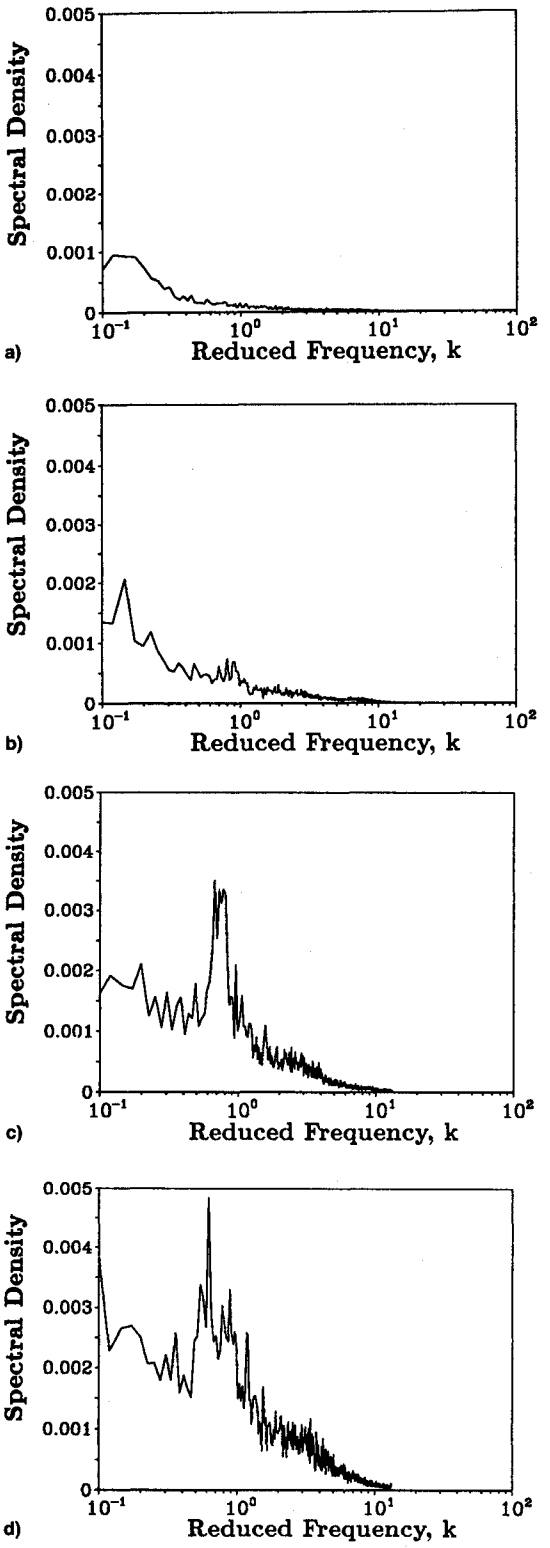

Fig. 12 Spectra of the lateral velocity component v at station 4 (plane of symmetry) at $Z = 0.21$ for various angles of attack: a) $\alpha = 20$ deg, $v_{rms}/U_\infty = 1.1\%$; b) $\alpha = 25$ deg, $v_{rms}/U_\infty = 1.5\%$; c) $\alpha = 28$ deg, $v_{rms}/U_\infty = 2.3\%$; and d) $\alpha = 30$ deg, $v_{rms}/U_\infty = 3.0\%$.

For a single fin located at the wing midsection the turbulence level normal to the fin is much smaller (≈4%) compared with twin-fin configurations (≈20%) located at $Y = \pm 0.11$ for instance. This may be different if the aircraft is operated at some angle of sideslip. For that condition the vortex system is shifted to the midsection. Turbulence levels at single fin and twin-fin might not differ susbstantially in that case.

Summarizing, Fig. 9 gives a schematic overview of the cross-sectional wing flowfield and its turbulence level at moderate and high angles of attack. They are shown for a spanwise and a vertical line through the vortex core. For moderate angles of attack ($\alpha \approx 15$ deg, Fig. 9a), the leading-edge vortices are concentrated outboard. The rms profiles show the two peaks corresponding to the vortex sheet and a local rms drop in the vortex core. Steep gradients indicate the inboard and outboard vortex sheet. In the midsection the turbulence level is the lowest one. A fundamental change occurs in the flowfield if the angle of attack is increased to $\alpha \approx 30$ deg. The leading-edge vortices move inboard, accompanied by a strong expansion of the vortex core due to vortex bursting. Thus, the turbulence levels are also markedly increased. The midsection remains, however, still the locus of minimum turbulence levels.

Spectral Analysis

For a single fin mainly the lateral flowfield velocity causes buffeting, whereas for a twin-fin with dihedral, both the lateral and the vertical velocity contribute. Spectral analysis gives the magnitude and the frequencies for the buffeting excitation levels.

Character of the Spectral Content at High Angle of Attack

Figure 10 shows the stations for which the velocity spectra have been evaluated. Results are shown for $\alpha = 28$ deg only, and give a general view of the distribution of kinetic turbulent energy at high α. Six single density spectra plots and two staggered spectra plots both on the left and right side of the cross section are shown in Fig. 11.

The velocity spectra in Figs. 11a and 11d are related to stations left and right of the midsection. For these locations corresponding to the wing primary vortex core the spectra have a pronounced broad frequency hump ranging from $k = 0.54$ to $k = 1.17$. The turbulence level reaches values of 12.4 and 13.9% based on freestream velocity.

At stations 2l and 2r (Figs. 11b and 11e), however, a strong narrow-band frequency peak which is closely associated with

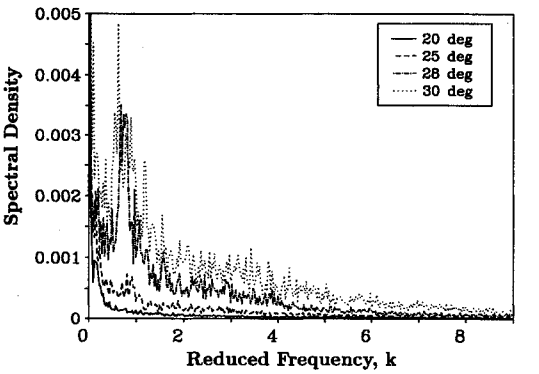

Fig. 13 Comparison of the v-velocity spectra at station 4 (plane of symmetry, $Z = 0.21$) for various angles of attack.

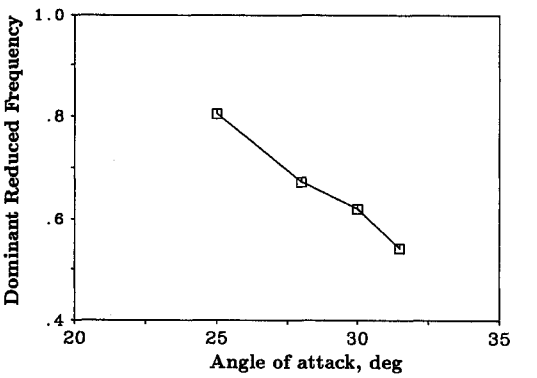

Fig. 14 Reduced frequency of the dominant peak as a function of angle of attack measured at station 4, $Z = 0.21$.

the pronounced velocity fluctuations in the vortex sheet is observed. The turbulence level reaches values of approximately 11%. From Figs. 11b and 11e it appears that the spectral energy is accumulated in this limited frequency range. This may indicate a periodic or quasiperiodic fluctuation which is due to the swirling vortex pattern. Roughly 75% of the turbulent energy is concentrated within this narrow band.

The power spectrum density values for stations 3l and 3r near the midsection are appreciably small (Figs. 11c and 11f). The kinetic turbulent energy decreases by an order of magnitude, but the spectra show a concentration of kinetic turbulent energy in the specified frequency range again. It is obvious that by the induced concentration of turbulent energy into a limited frequency range the vortex sheet affects the flow conditions even in the plane of symmetry.

Further on the power spectrum density increases strongly in the spanwise direction (Figs. 11g and 11h), that is directly related to the vortex shear layer and core position. The turbulent energy is mainly concentrated within $k = 0.72 \div 1.17$.

Variation of Frequency Content with Angle of Attack

Figure 12 shows spectra for various angles of attack at station 4 (plane of symmetry). Up to 20 deg, Fig. 12a, a broadband spectrum may excite normal, random buffeting. From Figs. 6b and 7b it appears that no vortex sheet influences the midsection at that angle of attack. At $\alpha = 25$ deg, the spectral content becomes quite different. Figure 12b shows a spectrum with low turbulence level, but sharp peaks occur around a hump of $k = 0.9$. Regarding the midsection this hump cannot be detected at a lower angle of attack. A dramatic change occurs in the spectral density at $\alpha = 28$ deg, Fig. 12c. A distinct narrow-band frequency peak centered around $k = 0.75$ predominates the whole spectrum. It indicates that the spectral energy has been channeled into this narrow band. The dominant frequency peak in the spectrum of Fig. 12c corresponds with the sharp frequency peak of the vortex sheet spectra which are discussed in Figs. 11b and 11e, respectively. At $\alpha = 30$ deg (Fig. 12d), the spectrum becomes widened around $k = 0.68$ with multiple peaks.

In the high-α domain the narrow-band concentration of kinetic turbulent energy associated with the strong fluctuation intensity in the joined vortex sheets of wing and canard is extended to the plane of symmetry. This is caused by the inboard leading-edge vortex shift together with the growth of burst vortices, Figs. 6c and 6d and Figs. 7c and 7d. (Note that the ordinate of Fig. 12 is scaled smaller by one order in magnitude than the ordinate of Fig. 11.)

In Fig. 13 the spectra of Figs. 12a–12d are compared. With increasing angle of attack the frequency of the dominant peak decreases. This is summarized in Fig. 14. Even using a linear scale, there is some ambiguity in the determination of the dominant peak because of single spikes centered around a broader hump. As observed previously[10,17] at different angles of attack the peaks of the buffeting spectrum may move into the range of different structural modes, resulting in a "tuning" of the vibrations. This is because of fluctuations associated with the bursting of strong leading-edge vortices.

Scaling to Full Scale

Using k, the dominant peak can be scaled to full scale. The assumption would be, that the leading-edge flow separation line is fixed, and consequently it is not very dependent on Reynolds number.

Conclusions

The time-average and rms of the velocity components in a turbulent flowfield caused by a vortex-dominated configuration have been studied from moderate to high angles of attack using hot-wire anemometry. The frequency contents of the fluctuating flowfield are also presented. Major results of these investigations are as follows:

1) Already at moderate angles of attack ($\alpha \approx 15$ deg) the vortex systems of wing and canard are strongly influenced by dissipation giving an increase in the turbulence levels.

2) When the angle of attack is increased, the delta wing vortex system moves inboard towards the midsection and upwards. The vortices grow continuously in their radial extension, leading to a large vortex core. This is emphasized by a strong decrease of the axial- and azimuthal velocity due to vortex bursting.

3) The burst vortex flowfield shows a strong increase of the turbulence level for all three velocity components. Steep gradients separate the vortex sheet region from the outer flowfield. The maxima of rms values shows an annular structure which is attributed to the vortex sheet, while in the vortex core a local rms decrease occurs.

4) At angle of attack the enlarged wing primary vortices generate a strong nozzle effect in the plane of symmetry. They induce large additional velocities and lower turbulence levels.

5) For moderate angles of attack ($\alpha < 20$ deg) it is shown that above the wing through wing influence the canard vortex-system is moved towards the midsection and also downward towards the wing. At an angle of attack ($\alpha \approx 20$ deg) the interaction between the wing and canard vortex systems makes the canard trailing-vortex sheet move upwards, whereas the canard leading-edge vortex sheet merges with the wing primary vortex. Thus, a local maximum in the turbulence level is found near the root of a possible single fin.

6) The spectra of the vortex sheets show a distinct narrow-band peak, whereas the vortex core region depicts a broader frequency hump. The narrow-band concentration of kinetic turbulent energy indicates a strong periodicity in the flow.

7) With increasing angle of attack this narrow-band turbulent energy affects the plane of symmetry because of vortex shift and enlarged vortex cores. In the midsection at 25-deg angle of attack firstly a concentration of turbulent energy in a limited frequency range is observed. At $\alpha = 28$ deg a distinct sharp peak occurs dominating the whole spectrum.

8) Depending on the angle of attack the frequency of the peak and the shape of the spectrum is changed.

9) For symmetric flow conditions a single fin usually will show much less buffeting excitation when compared with a twin-fin arrangement. This may alter under sideslip conditions and a detailed investigation on the optimum fin locations might be required. It is thought that the present investigation will give useful insight into this question.

Acknowledgments

This work was supported by MESSERSCHMITT–BÖLKOW–BLOHM GmbH, now DASA, under the directorat of W. Schmidt. The authors express their appreciation to J. Becker (DASA) for initiating the investigation and for his continuous advice and kind assistance.

References

[1]Mabey, D. G., "Beyond the Buffet Boundary," *Aeronautical Journal*, Vol. 11, No. 148, 1973, pp. 201–214.

[2]Becker, J., "Bewegungsinduzierte Luftkräfte bei abgelöster Strömung und ihre Übertragung auf die Ermittlung der Strukturresponse," Ph.D. Dissertation, Technische Univ. Braunschweig, Braunschweig, Germany, 1982.

[3]Blenk, H., Fuchs, D., and Liebers, F., "Über Messungen von Wirbelfrequenzen," *Luftfahrtforsch.*, Bd. 12, 1935, pp. 38–41.

[4]Mabey, D. G., and Pyne, C. R., "Fin Buffeting at High Angles of Incidence on a Model of Slender Wing Aircraft," International Forum on Aeroelasticity and Structural Dynamics, Paper 91-129, Aachen, Germany, June 1991, pp. 552–561.

[5]Ashley, H., Rock, S. M., Eggers, A. J., Jr., Digumarthi, R. V., and Chaney, K., "Active Control for Fin Buffet Alleviation," Mid-Year Rept., RANN, Palo Alto, CA, Jan. 1993.

[6]Brown, D., Lee, B. H. K., and Tang A., "Some Characteristics and Effects of the F/A-18 Lex Vortices," *Vortex Flow Aerodynamics*, AGARD Paper 30 CP-494, Scheveningen, The Netherlands, Oct. 1990, pp. 30-1–30-20.

[7]Lee, B. H. K., and Brown, D., "Wind-Tunnel Studies of F/A-18 Tail Buffet," *Journal of Aircraft*, Vol. 29, No. 1, 1992, pp. 146–152.

[8]Triplett, W. E., "Pressure Measurements on Twin Vertical Tails in Buffeting Flow," *Journal of Aircraft*, Vol. 20, No. 11, 1983, pp. 920–925.

[9]Erickson, G. E., Hall, R. M., Banks, D. W., Del Frate, J. H., Schreiner, J. A., Hanley, R. J., and Pulley, C. T., "Experimental Investigation of the F/A-18 Vortex Flows at Subsonic Through Transonic Speeds, Invited Paper," AIAA Paper 89-2222, July–Aug. 1989.

[10]Wentz, W. H., "Vortex-Fin Interaction on a Fighter Aircraft," AIAA Paper 87-2474, Aug. 1987.

[11]Lee, B. H. K., Brown, D., Zgela, M., and Poirel, D., "Wind Tunnel Investigation and Flight Tests of Tail Buffet on the CF-18 Aircraft," *Aircraft Dynamic Loads Due to Flow Separation*, Paper 1 (Sorrento, Italy), 1990, pp. 1-1–1-26 (AGARD CP-483).

[12]Sellers, W. L., Meyers, J. F., and Hepner, T. E., "LDV Surveys over a Fighter Model at Moderate to High Angles of Attack," Society of Automotive Engineers TP Series Paper 88-1448, Oct. 1988.

[13]Komerath, N. M., Liou, S. G., Schwartz, R. J., and Kim, J. M., "Flow over a Twin-Tailed Aircraft at Angle of Attack, Part I: Spatial Characteristics," *Journal of Aircraft*, Vol. 29, No. 3, 1992, pp. 413–420.

[14]Komerath, N. M., Liou, S. G., Schwartz, R. J., and Kim, J. M., "Flow over a Twin-Tailed Aircraft at Angle of Attack, Part II: Temporal Characteristics," *Journal of Aircraft*, Vol. 29, No. 4, 1992, pp. 553–558.

[15]Lee, B. H. K., "A Method for Predicting Wing Response to Buffet Loads," *Journal of Aircraft*, Vol. 21, No. 1, 1984, pp. 85–87.

[16]Lee, B. H. K., and Dunlavy, S., "Statistical Prediction of Maximum Buffet Loads on the F/A-18 Vertical Fin," *Journal of Aircraft*, Vol. 29, No. 4, 1992, pp. 734–736.

[17]Zimmermann, N. H., Ferman, M. A., Yurkovich, R. N., and Gerstenkorn, G., "Prediction of Tail Buffet Loads for Design Applications," AIAA Paper 89-1378, April 1989.

[18]Lan, C. E., and Lee, I. G., "Investigation of Empennage Buffeting," NASA CR-179246, Jan. 1986.

[19]Johnson, F. D., and Eckelmann, H., "A Variable Angle Method of Calibration for X-Probes Applied to Wall-Bounded Turbulent Shear Flow," *Experiments in Fluids*, Vol. 3, No. 2, 1984, pp. 121–130.

[20]Lueptow, R. M., Breuer, K. S., and Haritonidis, J. H., "Computer-Aided Calibration of X-Probes Using a Look-Up Table," *Experiments in Fluids*, Vol. 7, No. 6, 1988, pp. 115–118.

[21]Samet, M., and Einav, S., "A Hot-Wire Technique for Simultaneous Measurement of Instantaneous Velocities in 3D Flows," *Journal of Physics E: Scientific Instruments*, Vol. 20, 1987, pp. 683–690.

[22]Browne, L. W. B., Antonia, R. A., and Chua, L. P., "Calibration of X-Probes for Turbulent Flow Measurements," *Experiments in Fluids*, Vol. 8, No. 7, 1989, pp. 201–208.

[23]Breitsamter, C., "Messungen und Analyse der zeitabhängigen Geschwindigkeiten im wirbeldominierten Strömungsfeld eines Hochleistungsflugzeuges, Teil 1," FLM-91/22, Lehrstuhl für Fluidmechanik, Technische Universität München, Munich, Germany, 1991.

"Random [24]Bendat, J. S., and Piersol, A. G., *Random Data: Analysis and Measurement Procedures*, Wiley, New York, 1971.

[25]Breitsamter, C., "Messungen und Analyse der zeitabhängigen Geschwindigkeiten im wirbeldominierten Strömungsfeld eines Hochleistungsflugzeuges, Teil 2," FLM-91/54, Lehrstuhl für Fluidmechanik, Technische Universität München, Munich, Germany, 1991.

[26]Breitsamter, C., "Sichtbarmachung von Wandschubspannungen mit Hilfe schubspannungssensitiver Flüssigkristalle," FLM-93/4, Lehrstuhl für Fluidmechanik, Technische Univ. München, Munich, Germany, 1993.

[27]Oelker, H.-Chr., "Aerodynamische Untersuchungen an kurzgekoppelten Entenkonfigurationen bei symmetrischer Anströmung," ZLR-Forschungsbericht 90-01, Technische Universität Braunschweig, Braunschweig, Germany, 1990.